# Simulation of copper–water nanofluid in a microchannel in slip flow regime using the lattice Boltzmann method

Arash Karimipour [a,*], Alireza Hossein Nezhad [b], Annunziata D'Orazio [c], Mohammad Hemmat Esfe [a], Mohammad Reza Safaei [d], Ebrahim Shirani [e]

[a] Department of Mechanical Engineering, Najafabad Branch, Islamic Azad University, Isfahan, Iran
[b] Department of Mechanical Engineering, University of Sistan and Baluchestan, Zahedan, Iran
[c] Dipartimento di Ingegneria Astronautica, Elettrica ed Energetica, Sapienza Università' di Roma, Via Eudossiana 18, Roma 00184, Italy
[d] Young Researchers and Elite Club, Mashhad Branch, Islamic Azad University, Mashhad, Iran
[e] Foolad Institute of Technology, Fooladshahr, Isfahan, Iran

## ARTICLE INFO

## ABSTRACT

Laminar forced convection heat transfer of water–Cu nanofluids in a microchannel was studied utilizing the lattice Boltzmann method (LBM). The entering flow was at a lower temperature compared to the microchannel walls. Simulations were performed for nanoparticle volume fractions of 0.00 to 0.04 and slip coefficient from 0.005 to 0.02. The model predictions were found to be in good agreement with earlier studies. The effects of wall slip velocity and temperature jump of the nanofluid were studied for the first time by using lattice Boltzmann method. Streamlines, isotherms, longitudinal variations of Nusselt number, slip velocity and temperature jump as well as velocity and temperature profiles for different cross sections were presented. The results indicate that LBM can be used to simulate forced convection for the nanofluid micro flows. Moreover, the effect of the temperature jump on the heat transfer rate is significant. Also, the results showed that decreasing the values of slip coefficient enhances the convective heat transfer coefficient and consequently the Nusselt number (Nu) but increases the wall slip velocity and temperature jump values.

## 1. Introduction

During the last two decades, much attention has been paid to make and use micro devices. The small sizes as well as high efficiency of micro devices – such as microsensors, microvalves and micropumps – are some of the advantages of using MEMS and NEMS (Micro and Nano Electro Mechanical Systems). To guarantee the performance of such devices and make them cool, many studies have been carried out concerning flow and heat transfer in microchannels. At micro scale level, the surface effects are getting more important which leads to change in the classic boundary conditions. The well known differences of micro flows from the macroscopic ones are the slip velocity and temperature jump on the solid–fluid boundaries. For the gas micro flows, the flow regimes can be slip, transient and free molecular flow regimes; however for liquid micro flows, mainly the slip flow regime can be observed [1–9]. Therefore, in addition to classic Navier–Stokes (NS), the particle-based methods including direct simulation of Monte Carlo (DSMC), molecular dynamics (MD) and the lattice Boltzmann method (LBM) may be applied [10,11]. Expensive computation cost and complex mathematical procedure of MD and DSMC, as well as the inability of N–S for simulation of flow in transition and free molecular regimes, have encouraged the researchers to use LBM [12–20].

In LBM, the fluid flow is simulated by the collision and streaming of fictive particles on the lattice nodes. The collision rule is approximated mainly by the BGK model which is the most popular model in LBM studies [21]. LBM uses the simple parallel algorithms and deals appropriately with the complex boundaries, and describes the flow parameters in micro and nano scales well. Succi [22] and Chen et al. [23,24] have done appropriate studies to show the LBM appropriate performance. There are some different thermal LBM models. Among them, the internal energy

* Corresponding author. Tel.: +98 9133251252.
*E-mail addresses:* arashkarimipour@gmail.com, arash.karimipour@uniroma1.it, arash.karimipour@pmc.iaun.ac.ir (A. Karimipour), Nezhadd@hamoon.usb.ac.ir (A. Hossein Nezhad), annunziata.dorazio@uniroma1.it (A. D'Orazio), M.hemmatesfe@gmail.com (M. Hemmat Esfe), cfd_safaei@yahoo.com (M.R. Safaei), eshirani@ictp.it (E. Shirani).

## Nomenclature

| | |
|---|---|
| $B = \beta/h$ | Dimensionless slip coefficient |
| $\mathbf{c} = (c_x, c_y)$ | Microscopic velocity vector |
| $C_p$ | Heat capacity, J kg$^{-1}$ K$^{-1}$ |
| $D_H = 2h$ | Hydraulic diameter, m |
| $d_f$ | Molecular diameter of the base fluid, nm |
| $d_p$ | Nanoparticle diameter, nm |
| $e$ | Internal energy density |
| $f, g$ | Distribution functions for density–momentum and internal energy |
| $\tilde{f}_i, \tilde{g}_i$ | Modified discrete distribution functions |
| $h, l$ | Microchannel height and length, m |
| $H, L$ | Dimensionless height and length of the microchannel |
| $k$ | Thermal conductivity coefficient, W m$^{-1}$ K$^{-1}$ |
| Kn | Knudsen number |
| $L_s$ | Slip length, m |
| $l_{BF}$ | Mean free path of the base fluid, nm |
| Nu | Local Nusselt number at the outlet |
| Nu$_X$ | Local Nusselt number along the microchannel wall |
| Pr $= \upsilon_{nf}/\alpha_{nf}$ | Prandtl number |
| $r$ | Accommodation coefficient (in Eq. (28)) |
| $R$ | Gas constant |
| Re $= \rho_{nf} u_{nf} D_H/\mu_{nf}$ | Reynolds number |
| $t$ | Time, s |
| $T$ | Temperature, K |
| $T_c, T_h$ | Cold and hot temperatures, K |
| $T_i$ | Inlet temperature, K |
| $T_w$ | wall temperature, K |
| $\mathbf{u} = (u, v)$ | Macroscopic flow velocity vector, m s$^{-1}$ |
| $(U, V) = (u/u_i, v/u_i)$ | Dimensionless flow velocity in $x$–$y$ direction |
| $u_i$ | Inlet flow velocity, m s$^{-1}$ |
| $U_s$ | Slip velocity |
| $x, y$ | Cartesian coordinates, m |
| $(X, Y) = (x/h, y/h)$ | Dimensionless coordinates |
| $Z_i$ | Discrete heat dissipation |

*Greek symbols*

| | |
|---|---|
| $\alpha$ | Thermal diffusivity m$^2$ s$^{-1}$ |
| $\beta$ | Slip coefficient |
| $\varphi$ | Nanoparticles' volume fraction |
| $\mu$ | Dynamic viscosity, Pa s |
| $\theta = T/T_i$ | Dimensionless temperature |
| $\theta_s$ | Temperature jump |
| $\rho$ | Density, kg m$^{-3}$ |
| $\tau_f, \tau_g$ | Relaxation times for momentum and internal energy |
| $\zeta$ | Temperature jump distance |
| $\Omega$ | Collision operator |

*Super- and sub-scripts*

| | |
|---|---|
| $e$ | Equilibrium |
| $f$ | Base fluid (pure water) |
| $i$ | Inlet flow, Lattice directions |
| $nf$ | Nanofluid |
| $out$ | Outlet flow |
| $s$ | Solid nanoparticles |
| $w$ | Wall |
| $\alpha$ | $x$–$y$ geometry components |

distribution function presented by He et al. [25] is the most stable method and is able to consider the viscous heat dissipation and pressure work [26–28]. The new lattice Boltzmann methods such as Multi Relaxation Time lattice Boltzmann (MRT-LBM) show the researchers' interest to increase LBM performance at different conditions [29–33]. Regarding this, for instance, mixed convection heat transfer of air in a microchannel studied by Karimipour et al. [34].

On the other hand, using nanofluids is an innovative way to increase heat transfer which has attracted the researchers' interests who are working on micro flow due to their exciting potential. Nanofluids are a mixture of liquid and dispersed solid nanoparticles. The higher thermal conductivity of nanoparticles leads to the increase of nanofluid heat transfer. Nanofluid's characteristics are different from the traditional solid–liquid mixtures in milli or micro-meter particle's size. There are many studies concerning nanofluid in cavities and tubes which involve its positive effects on the Nusselt number [35–40]. For instance, Karimipour et al. [41] investigated the effect of Cu/water nanofluid on mixed convection in a cavity with sinusoidal top lid.

Nanofluid also has shown appropriate performance in macro scales [42,43]. Some researchers have reported the flow and heat transfer of the nanofluid in microchannels [44–47]. For instance, Raisi et al. [48] simulated the Cu–water nanofluid in a microchannel for both slip and no-slip conditions, ignoring the temperature jump effects and applying the classic Navier–Stokes equations. All in all, theoretical results of fluid flow in slip flow regimes or even simulation of nanofluid flow using LBM (in single phase or multi-phase mixture model) have been presented by several researchers [49–54]. However, there are few studies concerning nanofluid simulation in microchannels using LBM [55,56]. However, all of them have ignored the slip velocity and temperature jump effects. In addition, in most of the previous works, using classic Navier–Stokes equations, the temperature jump has not been considered in the simulations.

The presented literature survey suggests that nanofluids are an effective coolant which requires more investigations. In particular, the convection heat transfer of nanofluids in microchannel in the slip flow regime as well as the effect of temperature jump is still not entirely understood. In the present study, laminar forced convection heat transfer of dilute water–Cu nanofluids in a microchannel is analyzed. The flow regime's simulation results were weighed against model validation results found in the literature. Particular attention was paid to the effects of temperature jump and slip velocity in laminar forced convection of water/Cu nanofluids with different solid volume fractions in the slip flow regime using the lattice Boltzmann method.

## 2. Problem statement

Forced convection heat transfer of the nanofluid in a two dimensional microchannel as shown in Fig. 1 is studied numerically, using double population LBM–BGK. In this method, hydrodynamic and thermal parameters of fluid flow are estimated using the density–momentum distribution function, $f$, and the internal energy density distribution function, g, respectively.

The velocity and temperature profiles at the inlet are considered as $u_i$ and $T_i$. The wall temperature is set to $T_w = 2T_i$. As the length of the microchannel is long enough and fully developed hydrodynamic and thermal conditions are obtained rapidly, therefore, Re is small. Regarding this, in the present study the Reynolds number is set to Re $= 0.01$.

The nanofluid simulated in this work is a dispersion of nanoparticles of copper (Cu) in pure water (as the base liquid). It is assumed that the considered fluid is a Newtonian, incompressible fluid, in laminar flow regime. Nanoparticles are spherical with diameter as
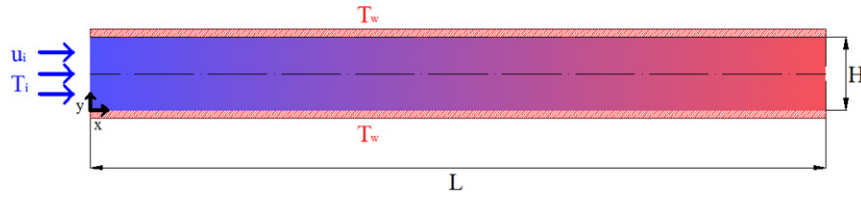
**Fig. 1.** The schematic diagram of the microchannel.

$d_p = 10$ nm. Water and nanoparticles mixture is in the homogeneous mode and the radiation effect is negligible.

The effects of different values of nanoparticle volume fraction ($\varphi = 0$, $\varphi = 0.02$ and $\varphi = 0.04$) are investigated for forced convection of nanofluid in a microchannel. Moreover, the slip velocity and temperature jump and their effects are studied for different values of slip coefficient as $B = 0.005$, $B = 0.01$ and $B = 0.02$.

## 3. Formulation

### 3.1. Nanofluid

Nanofluid is a homogeneous mixture of the liquid and suspended nanoparticles. Its effective density can be obtained by:

$$\rho_{nf} = \varphi \rho_s + (1 - \varphi)\rho_f \tag{1}$$

where $\varphi$ is the nanoparticle volume fraction and the subscripts $f$, $s$ and $nf$ refer to base fluid, solid nanoparticles and nanofluid, respectively.

Using the heat capacity of nanofluid, the nanofluid thermal diffusivity can be obtained by [57]:

$$(\rho C_p)_{nf} = (1 - \varphi)(\rho C_p)_f + \varphi(\rho C_p)_s \tag{2}$$

$$\alpha_{nf} = k_{nf}/(\rho C_p)_{nf}. \tag{3}$$

The effective dynamic viscosity is expressed by using the Brinkman model [58]:

$$\mu_{nf} = \mu_f/(1 - \varphi)^{2.5}. \tag{4}$$

Eq. (5), which was presented by Chon et al. [59], is considered to determine the nanofluid thermal conductivity:

$$\frac{k_{nf}}{k_f} = 1 + 64.7 \times \varphi^{0.7460} \left(\frac{d_f}{d_p}\right)^{0.3690} \left(\frac{k_s}{k_f}\right)^{0.7476}$$

$$\times \left(\frac{\mu}{\rho_f \alpha_f}\right)^{0.9955} \left(\frac{\rho_f B_c T}{3\pi \mu^2 l_{BF}}\right)^{1.2321} \tag{5}$$

in which

$$\mu = A \times 10^{\frac{B}{T-C}}, \qquad C = 140 \text{ (K)}, \tag{6}$$

$$B = 247.8 \text{ (K)}, \qquad A = 2.414 \times 10^{-5} \text{ (Pa s)}.$$

Eq. (5) is able to take into account the nanoparticles diameter and their Brownian motion. $B_c$ shows the Boltzmann constant ($1.3807 \times 10^{-23}$ J/K) and $l_{BF}$ represents the base fluid mean free path.

### 3.2. Lattice Boltzmann method

The hydrodynamic and thermal Boltzmann equations are written as follows [60]:

$$\frac{\partial f_i}{\partial t} + c_{i\alpha} \frac{\partial f_i}{\partial x_\alpha} = \Omega(f) = -\frac{1}{\tau_f}(f_i - f_i^e) \tag{7}$$

$$\frac{\partial g_i}{\partial t} + c_{i\alpha} \frac{\partial g_i}{\partial x_\alpha} = \Omega(g_i) - f_i Z_i = 0.5 |\mathbf{c} - \mathbf{u}|^2 \Omega(f_i) - f_i Z_i$$

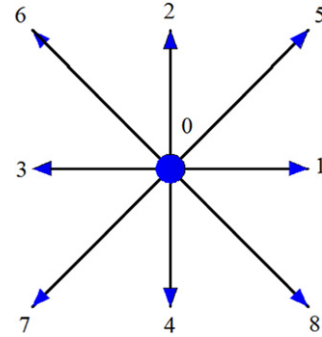$$= -\frac{g_i - g_i^e}{\tau_g} - f_i Z_i \tag{8}$$



**Fig. 2.** D2Q9 lattice.

where $\mathbf{u} = (u, v)$ and $\Omega$ are the macroscopic velocity vector and collision operator, respectively. $f$ and $g$ are distribution functions for density–momentum and internal energy. $f^e$ and $g^e$ are the equilibrium distribution functions and $\mathbf{c}_i$ indicates the microscopic velocity scale. The hydrodynamic and thermal relaxation times are shown as $\tau_f$ and $\tau_g$; meanwhile the subscript $i$ indicates the lattice velocity directions and $\alpha$ expresses the $\mathbf{x} = (x, y)$ geometry components.

The D2Q9 lattice model (Fig. 2) is applied to present study [61]. According to this model, microscopic discretized velocities can be written as follows [62]:

$$\mathbf{c}_i = \left(\cos \frac{i-1}{2}\pi, \sin \frac{i-1}{2}\pi\right), \quad i = 1, 2, 3, 4$$

$$\mathbf{c}_i = \sqrt{2}\left(\cos\left[\frac{(i-5)}{2}\pi + \frac{\pi}{4}\right], \sin\left[\frac{(i-5)}{2}\pi + \frac{\pi}{4}\right]\right), \tag{9}$$

$$i = 5, 6, 7, 8$$

$$\mathbf{c}_0 = (0, 0).$$

The heat dissipation term and equilibrium distribution functions are expressed as follows:

$$Z_i = (c_{i\alpha} - u_\alpha)\left[\frac{\delta u_\alpha}{\delta t} + c_{i\alpha} \frac{\partial u_\alpha}{\partial x_\alpha}\right] \tag{10}$$

$$f_i^e = \omega_i \rho \left[1 + 3(\mathbf{c}_i \cdot \mathbf{u}) + \frac{9(\mathbf{c}_i \cdot \mathbf{u})^2}{2} - \frac{3\mathbf{u}^2}{2}\right],$$

$$i = 0, 1, \ldots, 8 \tag{11}$$

$$\omega_0 = 4/9, \qquad \omega_{1,2,3,4} = 1/9, \qquad \omega_{5,6,7,8} = 1/36$$

$$g_0^e = -\frac{2}{3}\rho e \mathbf{u}^2$$

$$g_{1,2,3,4}^e = \frac{1}{9}\rho e \left[1.5 + 1.5(\mathbf{c}_{1,2,3,4} \cdot \mathbf{u}) + 4.5(\mathbf{c}_{1,2,3,4} \cdot \mathbf{u})^2 - 1.5\mathbf{u}^2\right] \tag{12}$$

$$g_{5,6,7,8}^e = \frac{1}{36}\rho e \left[3 + 6(\mathbf{c}_{5,6,7,8} \cdot \mathbf{u}) + 4.5(\mathbf{c}_{5,6,7,8} \cdot \mathbf{u})^2 - 1.5\mathbf{u}^2\right].$$

The discretized forms of Eqs. (7) and (8) are written as:

$$f_i(\mathbf{x} + \mathbf{c}_i \Delta t, t + \Delta t) - f_i(\mathbf{x}, t)$$

$$= -\frac{\Delta t}{2\tau_f}\left[f_i(\mathbf{x} + \mathbf{c}_i \Delta t, t + \Delta t) - f_i^e(\mathbf{x} + \mathbf{c}_i \Delta t, t + \Delta t)\right]$$

$$-\frac{\Delta t}{2\tau_f}\left[f_i(\mathbf{x},t)-f_i^e(\mathbf{x},t)\right] \tag{13}$$

$$g_i(\mathbf{x}+\mathbf{c}_i\Delta t,t+\Delta t)-g_i(\mathbf{x},t)$$
$$=-\frac{\Delta t}{2\tau_g}\left[g_i(\mathbf{x}+\mathbf{c}_i\Delta t,t+\Delta t)-g_i^e(\mathbf{x}+\mathbf{c}_i\Delta t,t+\Delta t)\right]$$
$$-\frac{\Delta t}{2}f_i(\mathbf{x}+\mathbf{c}_i\Delta t,t+\Delta t)Z_i(\mathbf{x}+\mathbf{c}_i\Delta t,t+\Delta t)$$
$$-\frac{\Delta t}{2\tau_g}\left[g_i(\mathbf{x},t)-g_i^e(\mathbf{x},t)\right]-\frac{\Delta t}{2}f_i(\mathbf{x},t)Z_i(\mathbf{x},t). \tag{14}$$

Eqs. (13) and (14) are in implicit forms. To solve this difficulty, the new distribution functions $\tilde{f}_i$ and $\tilde{g}_i$ are introduced:

$$\tilde{f}_i=f_i+\frac{\Delta t}{2\tau_f}(f_i-f_i^e) \tag{15}$$

$$\tilde{g}_i=g_i+\frac{\Delta t}{2\tau_g}(g_i-g_i^e)+\frac{\Delta t}{2}f_iZ_i. \tag{16}$$

Using Eqs. (13)–(16) the collision and propagation steps in LBM are simulated as follows:

$$\tilde{f}_i(\mathbf{x}+\mathbf{c}_i\Delta t,t+\Delta t)-\tilde{f}_i(\mathbf{x},t)$$
$$=-\frac{\Delta t}{\tau_f+0.5\Delta t}\left[\tilde{f}_i(\mathbf{x},t)-f_i^e(\mathbf{x},t)\right] \tag{17}$$

$$\tilde{g}_i(\mathbf{x}+\mathbf{c}_i\Delta t,t+\Delta t)-\tilde{g}_i(\mathbf{x},t)$$
$$=-\frac{\Delta t}{\tau_g+0.5\Delta t}\left[\tilde{g}_i(\mathbf{x},t)-g_i^e(\mathbf{x},t)\right]-\frac{\tau_g\Delta t}{\tau_g+0.5\Delta t}f_iZ_i. \tag{18}$$

The hydrodynamic and thermal variables can be determined by [63]:

$$\rho=\sum_i\tilde{f}_i$$

$$\rho\mathbf{u}=\sum_i\mathbf{c}_i\tilde{f}_i \tag{19}$$

$$\rho e=\rho RT=\sum_i\tilde{g}_i-\frac{\Delta t}{2}\sum_if_iZ_i.$$

### 3.3. Inlet and outlet boundary conditions

Non-equilibrium bounce back model, normal to the boundary, is used for inlet and outlet hydrodynamic boundary conditions [64]. In this model, distribution functions are reflected in suitable ways to satisfy the equilibrium conditions and improve accuracy [65]. Eqs. (20) and (21) are used for inlet and outlet hydrodynamic boundary conditions using non-equilibrium bounce back model, respectively:

$$\tilde{f}_1=\tilde{f}_3+\frac{2}{3}\rho_iu_i$$

$$\tilde{f}_5=\tilde{f}_7+\frac{1}{2}(\tilde{f}_4-\tilde{f}_2)+\frac{1}{6}\rho_iu_i \tag{20}$$

$$\tilde{f}_8=\tilde{f}_6-\frac{1}{2}(\tilde{f}_4-\tilde{f}_2)+\frac{1}{6}\rho_iu_i$$

$$\tilde{f}_3=\tilde{f}_1-\frac{2}{3}\rho_{out}u_{out}$$

$$\tilde{f}_7=\tilde{f}_5-\frac{1}{2}(\tilde{f}_4-\tilde{f}_2)-\frac{1}{6}\rho_{out}u_{out}-\frac{1}{2}\rho_{out}v_{out} \tag{21}$$

$$\tilde{f}_6=\tilde{f}_8+\frac{1}{2}(\tilde{f}_4-\tilde{f}_2)-\frac{1}{6}\rho_{out}u_{out}+\frac{1}{2}\rho_{out}v_{out}.$$

The unknown inlet and outlet thermal distribution functions are estimated using the known inlet temperature profile and

non-equilibrium bounce back model as follow [26,27]:

$$\tilde{g}_5=\frac{6\rho e+3dt\sum_if_iZ_i-6(\tilde{g}_0+\tilde{g}_2+\tilde{g}_3+\tilde{g}_4+\tilde{g}_6+\tilde{g}_7)}{2+3u_i+3u_i^2}$$
$$\times[3.0+6u_i+3.0u_i^2]\frac{1}{36}$$

$$\tilde{g}_1=\frac{6\rho e+3dt\sum_if_iZ_i-6(\tilde{g}_0+\tilde{g}_2+\tilde{g}_3+\tilde{g}_4+\tilde{g}_6+\tilde{g}_7)}{2+3u_i+3u_i^2}$$
$$\times[1.5+1.5u_i+3.0u_i^2]\frac{1}{9} \tag{22}$$

$$\tilde{g}_8=\frac{6\rho e+3dt\sum_if_iZ_i-6(\tilde{g}_0+\tilde{g}_2+\tilde{g}_3+\tilde{g}_4+\tilde{g}_6+\tilde{g}_7)}{2+3u_i+3u_i^2}$$
$$\times[3.0+6u_i+3.0u_i^2]\frac{1}{36}$$

$$\tilde{g}_6=\frac{6(\tilde{g}_1+\tilde{g}_5+\tilde{g}_8)-3dt\sum_ic_{ix}Z_if_i-6\rho eu_{out}}{2-3u_{out}+3u_{out}^2}$$
$$\times[3.0-6.0u_{out}+6.0v_{out}+3.0u_{out}^2+3.0v_{out}^2$$
$$-9.0u_{out}v_{out}]\frac{1}{36}$$

$$\tilde{g}_3=\frac{6(\tilde{g}_1+\tilde{g}_5+\tilde{g}_8)-3dt\sum_ic_{ix}Z_if_i-6\rho eu_{out}}{2-3u_{out}+3u_{out}^2}$$
$$\times[1.5-1.5u_{out}+3.0u_{out}^2-1.50v_{out}^2]\frac{1}{9} \tag{23}$$

$$\tilde{g}_7=\frac{6(\tilde{g}_1+\tilde{g}_5+\tilde{g}_8)-3dt\sum_ic_{ix}Z_if_i-6\rho eu_{out}}{2-3u_{out}+3u_{out}^2}$$
$$\times[3.0-6.0u_{out}-6.0v_{out}+3.0u_{out}^2+3.0v_{out}^2$$
$$+9.0u_{out}v_{out}]\frac{1}{36}.$$

### 3.4. Microchannel walls boundary conditions

In the previous works where the no-slip regimes were considered, the boundary conditions have been considered as:

$$u_w=u_{liquid}\big|_w$$
$$T_w=T_{liquid}\big|_w \tag{24}$$

where $u_w$ and $u_{liquid}$ indicate the velocity of the wall and the velocity of the liquid on the wall, respectively. Similar definitions can be considered for temperature field. More studies showed the necessity of new slip boundary conditions for replacing with old ones to obtain more accuracy [66]. Thompson and Troian [67] provided molecular dynamics (MD) simulations to show the slip flow on the walls which was recalled the linear Navier boundary condition as:

$$\Delta u_w=u_{fluid}(y\to wall)-u_w=L_s\frac{\partial u_{fluid}(y)}{\partial y}\bigg|_w \tag{25}$$

where $L_s$ is the constant slip length. At high shear rates, the Navier condition fails and boundary condition will be nonlinear even though the liquid being still Newtonian. In the contrast, at low shear rates, the slip length has desired consistency with the Navier model. This phenomenon is just like the Knudsen number (Kn) rule for linear slip condition of Navier–Stokes equations in dilute gases ($\Delta U_w=\text{Kn}\partial U/\partial Y$). Ngoma and Erchiqui [68] considered $\beta$ for the
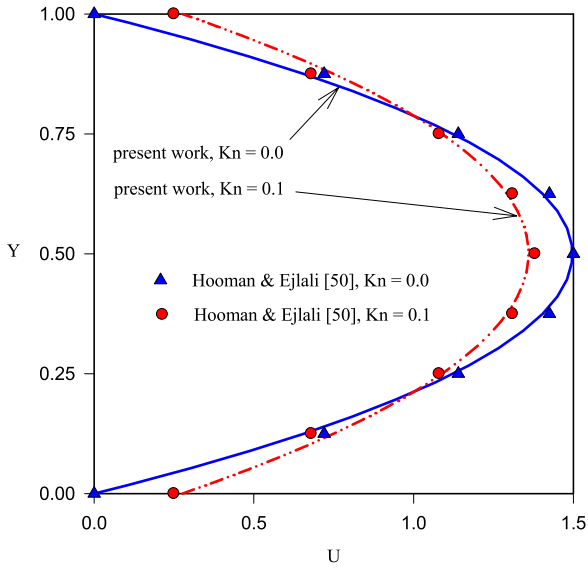
**Fig. 3.** Comparison of normalized fully developed velocity profiles and slip velocity along the microchannel walls with those of Hooman and Ejlali [50].
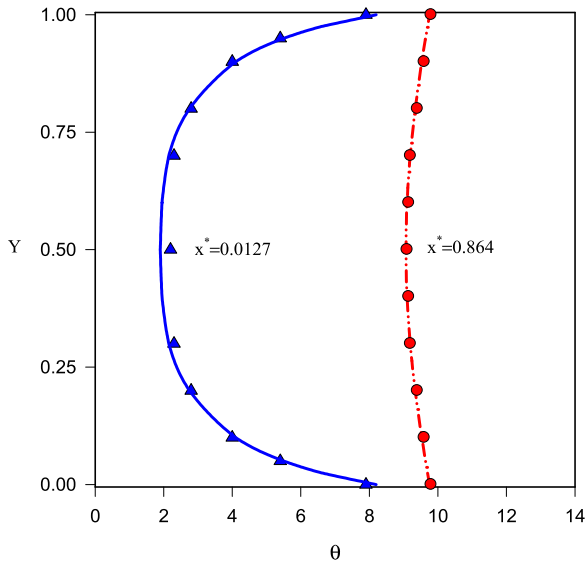


**Fig. 4.** Validation of dimensionless temperature profiles and temperature jump along the microchannel walls with the results of Kavehpour et al. [1] (lines: present work, symbols: Kavehpour et al. [1]).

slip length coefficient and defined the slip velocity for the liquid inside the microchannel on the stationary walls as follows:

$$u_s = \pm \beta \frac{\partial u}{\partial y}\Big|_{y=0,h} \tag{26}$$

where $u_s$ shows the liquid slip velocity on the wall. The non-dimensional form of Eq. (26) is written as:

$$U_s = \pm B \frac{\partial U}{\partial Y}\Big|_{Y=0,1}. \tag{27}$$

To determine the slip velocity utilizing Eq. (27) in LBM, the specular reflective bounce back model (combination of bounce back and specular boundary condition) is applied in this work. For example for the bottom wall, the unknown distribution functions are estimated by Eq. (28):

$$\tilde{f}_2 = \tilde{f}_4$$
$$\tilde{f}_{5,6} = r\tilde{f}_{7,8} + (1-r)\tilde{f}_{8,7}. \tag{28}$$
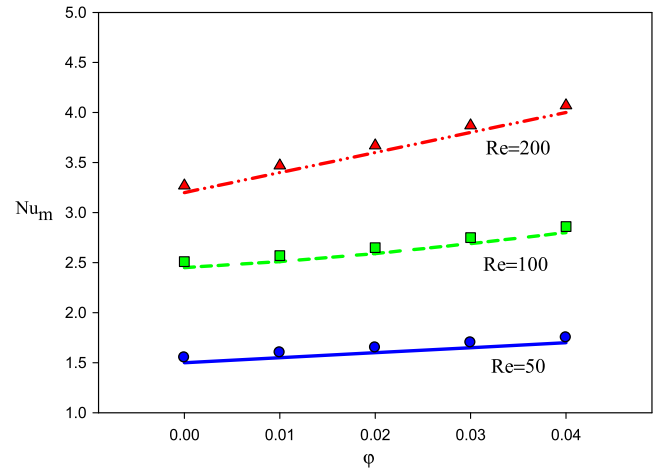


**Fig. 5.** Validation of present code with those of Santra et al. [36] for a nanofluid inside the channel (lines: present work, symbols: Santra et al. [36]).
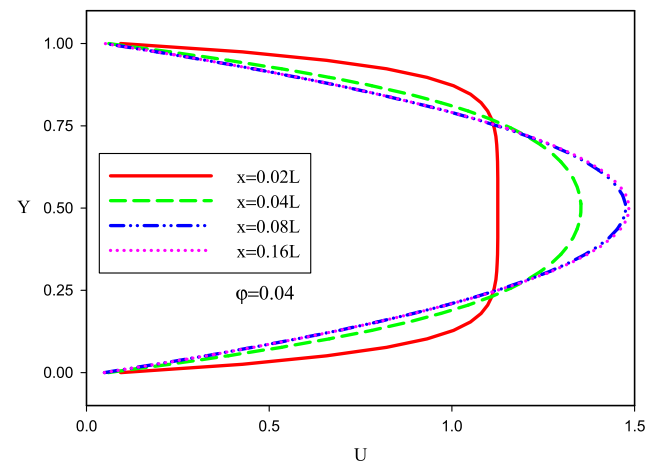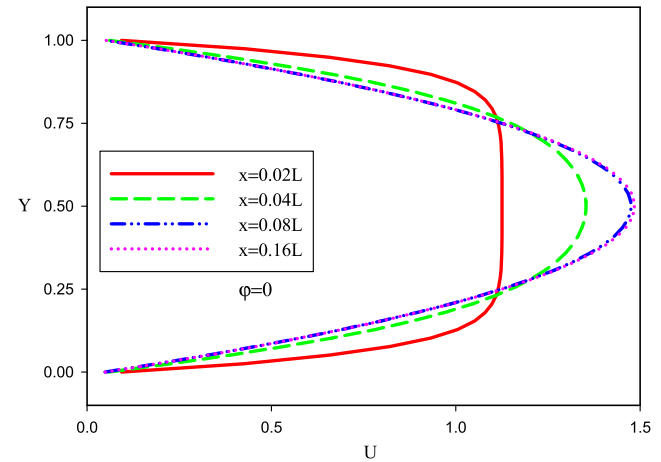




**Fig. 6.** Horizontal dimensionless velocity profiles, $U = u/u_i$, along the microchannel at $B = 0.005$ for $\varphi = 0$ and $\varphi = 0.04$.

The accommodation coefficient value, $r$, is chosen appropriately for more accuracy [69,70].

In analogy with the slip phenomenon, the temperature jump can be simulated on the microchannel walls by an equation as follows [71]:

$$\Delta T_w = T_{fluid}(y \to wall) - T_w = \zeta \frac{\partial T_{fluid}(y)}{\partial y}\Big|_w \tag{29}$$
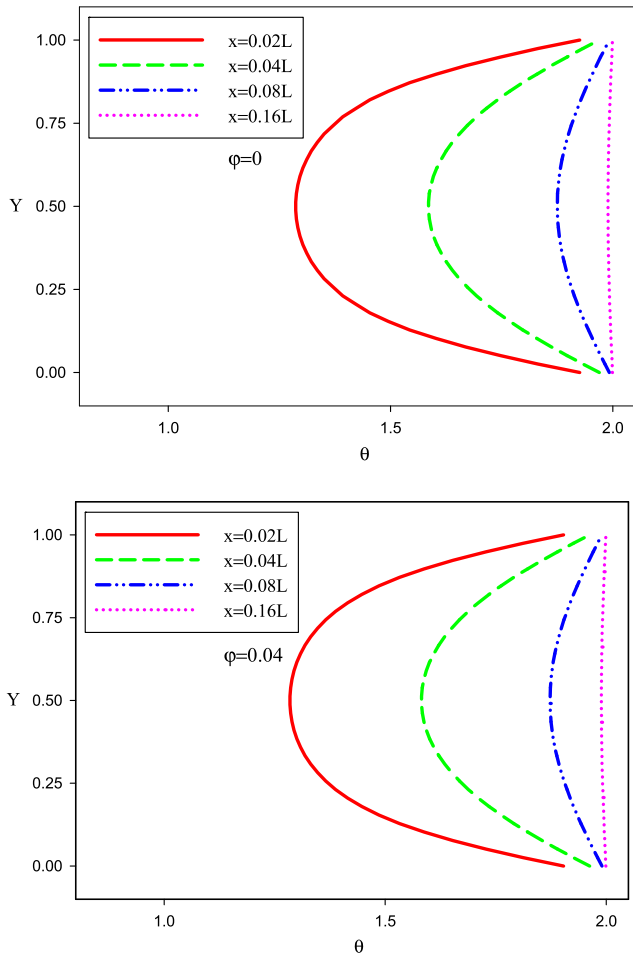
**Fig. 7.** Dimensionless temperature profiles, $\theta = T/T_i$, along the microchannel at $B = 0.005$ for $\varphi = 0$ and $\varphi = 0.04$.
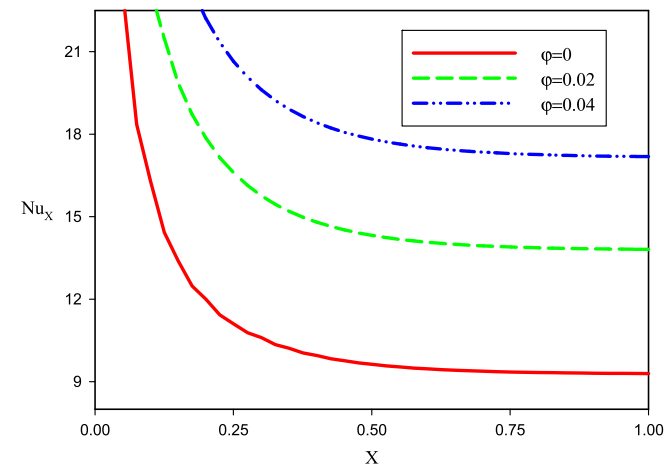


**Fig. 8.** $Nu_X$ along the microchannel wall at $B = 0.005$ for $\varphi = 0$, $\varphi = 0.02$ and $\varphi = 0.04$.
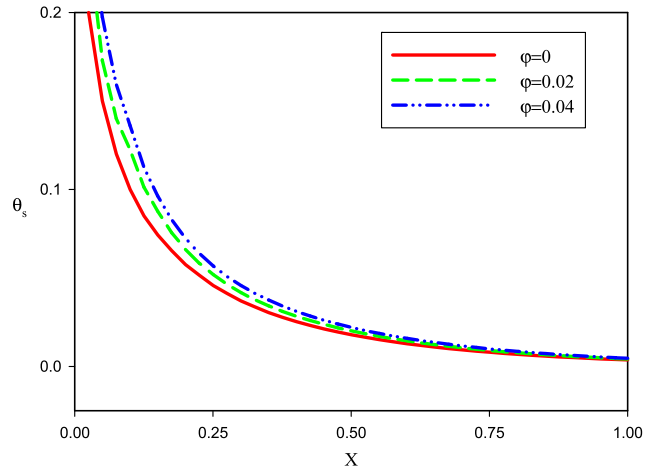


**Fig. 9.** $\theta_s$ along the microchannel wall at $B = 0.005$ for $\varphi = 0$, $\varphi = 0.02$ and $\varphi = 0.04$.



**Fig. 10.** $U$ along the microchannel at $B = 0.01$ and $B = 0.02$ for $\varphi = 0.04$.

where $\zeta$ is called the temperature jump distance. For dimensionless temperature at the wall, it can be obtained from Eq. (29):

$$\theta - \theta_w = \left. \frac{B}{\Pr} \frac{\partial \theta}{\partial Y} \right|_{Y=0,1}. \tag{30}$$

Using the diffuse scattering boundary condition (DSBC), the temperature jump for the bottom wall is written as below in LBM,

based on the internal energy distribution function [62]:

$$\tilde{g}_{2,5,6} = \frac{3}{\rho_w e} g^e_{2,5,6}(\rho_w, \mathbf{u}_w, e_w)(\tilde{g}_4 + \tilde{g}_7 + \tilde{g}_8). \tag{31}$$

The top wall temperature jump is also calculated similarly.

In the previous works where temperature jump of nanofluid has not been taken into account, the Nusselt number was usually defined as the functions of cold and hot temperatures as $Nu = k_{nf}/k_f$
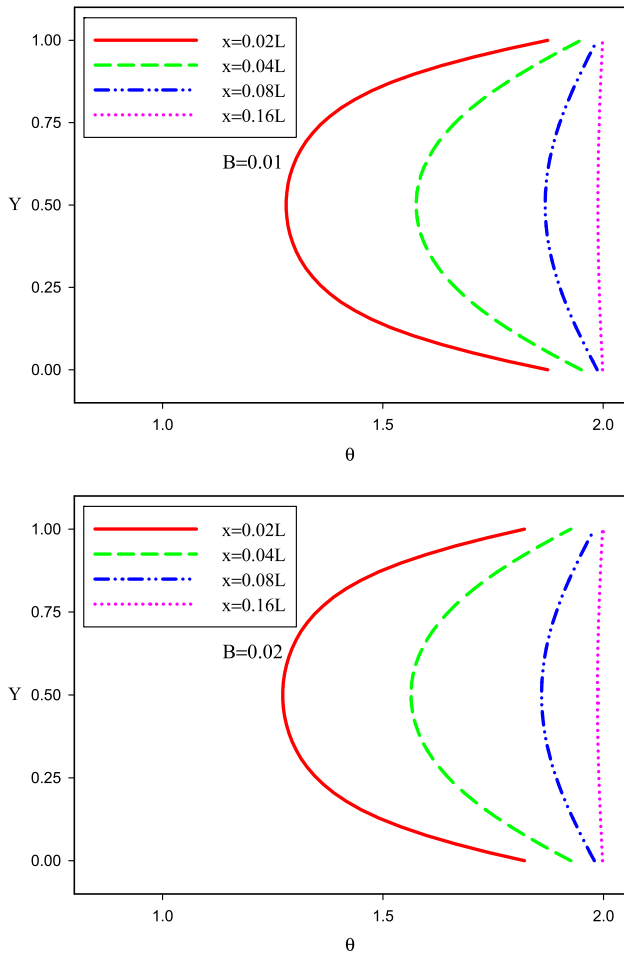
**Fig. 11.** $\theta$ along the microchannel at $B = 0.01$ and $B = 0.02$ for $\varphi = 0.04$.

**Table 1**
Grid independency for Re = 1, Pr = 0.7, $\varphi = 0$ and $B = 0.015$.

|  | $700 \times 35$ | $800 \times 40$ | $900 \times 45$ |
|---|---|---|---|
| Nu | 7.18 | 7.23 | 7.25 |
| $C_f$ Re | 21.04 | 21.10 | 21.13 |

outlet Nusselt number (Nu) at the outlet domain of a microchannel.

$$\text{Nu} = (k_{nf}/k_f) \frac{D_H \, (\partial T/\partial y)_w}{T_w - T_{bulk}}. \qquad (32)$$

## 4. Grid independency and validation

A FORTRAN LBM computer code is applied to study the flow and heat transfer of a nanofluid in a microchannel. Having studied grid independency for the code, as shown in Table 1, a lattice with $800 \times 40$ nodes is found appropriate for next computations.

For validation, first, ability of closed form solutions reported for slip velocity (Eqs. (27) and (28)) and temperature jump (Eqs. (30) and (31)) are examined in Figs. 3 and 4.

Fig. 3 shows the comparison of normalized fully developed velocity profiles and slip velocity on the walls with those of Hooman and Ejlali [50] for Kn = 0.0 and Kn = 0.1. Moreover the validation for dimensionless temperature profiles, $\theta = T/T_i$, and temperature jump value along the microchannel walls in comparison with the results of Kavehpour et al. [1] are shown in Fig. 4 for Re = 0.01, $T_w = 10$, $T_{inlet} = 1$, Pr = 0.7 and $Kn_{in} = 0.01$ and appropriate agreements are observed in both Figs. 3 and 4.

In addition, Niu et al. [62] considered a microchannel where its hot wall was cooled with an internal air flow at Re = 0.01. To have more validation with a micro flow, Table 2 shows the comparison of present results with those of Niu et al. [62] at Kn = 0.015, 0.02, 0.03, 0.04, 0.046.

The last selected case for validation is the forced convection of cold Cu–water nanofluid in a macro channel with hot walls which was studied by Santra et al. [36]. The averaged Nusselt number ($Nu_m$) against those of Santra et al. [36] is shown in Fig. 5 and good agreement is observed.

## 5. Results and discussions

The forced convection heat transfer of Cu–water nanofluid in a long microchannel is investigated by using LBM (Fig. 1).

$(\partial\theta/\partial Y)_w$ with $\theta = (T - T_c)/(T_h - T_c)$. However at present work, the effect of temperature jump (even a small value) results the temperature gradient between the wall and adjacent fluid layer. It means that Nu and the bulk temperature may be determined by considering Eq. (32). At this state, Nu approaches asymptotically to a constant value along the microchannel walls which is called the
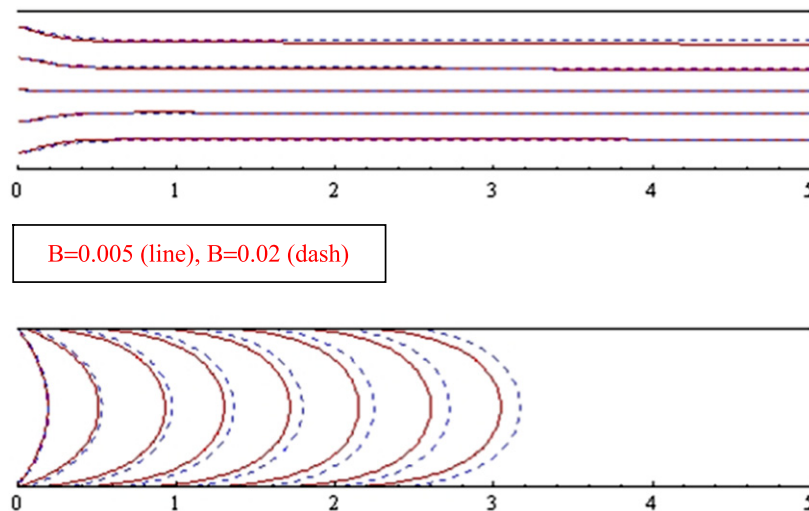


B=0.005 (line), B=0.02 (dash)

**Fig. 12.** Streamlines (top) and isotherms (bottom) of the nanofluid at $B = 0.005$ (line) and $B = 0.02$ (dash) for $\varphi = 0.04$.

**Table 2**
The validation of outlet Nu and $C_f$ Re at Re = 0.01 for air flow in microchannel.

|  | Kn = 0.015 | Kn = 0.02 | Kn = 0.03 | Kn = 0.04 | Kn = 0.046 |
|---|---|---|---|---|---|
| Nu [present work] | 7.23 | 7.20 | 7.09 | 6.78 | 6.63 |
| Nu [62] | 7.42 | 7.31 | 7.15 | 6.80 | 6.60 |
| $C_f$ Re [present work] | 21.10 | 20.81 | 19.48 | 18.63 | 18.01 |
| $C_f$ Re [62] | 21.49 | 21.15 | 19.75 | 18.85 | 18.20 |

**Table 3**
Thermophysical properties of Cu (copper) as the nanoparticles and water as the base fluid.

|  | $c_p$ (J/kg K) | $\rho$ (kg/m$^3$) | K (W/mK) | $\mu$ (Pa s) |
|---|---|---|---|---|
| Pure water | 4179 | 997.1 | 0.6 | $8.91 \times 10^{-4}$ |
| Cu | 383 | 8954 | 400 | – |

Thermophysical properties of Cu as the nanoparticles and water as the base fluid are presented in Table 3.

Reynolds number, Re $= \rho_{nf} u_{nf} D_H / \mu_{nf}$ and Prandtl number, Pr $= \upsilon_{nf}/\alpha_{nf}$ are calculated for the nanofluid mixture at $\varphi = 0\%$ (pure water), $\varphi = 0.02 = 2\%$ and $\varphi = 0.04 = 4\%$ using Eqs. (1)–(6).

### 5.1. Effects of nanoparticle concentration

Fig. 6 shows the horizontal dimensionless velocity profiles, $U = u/u_i$, along the microchannel wall at $B = 0.005$ for $\varphi = 0$ and $\varphi = 0.04$. The fully developed condition is observed at $x = 0.08$ L and $x = 0.16$ L after a short entrance length ($x = 0.02$ L and $x = 0.04$ L). Moreover, it can be seen that the nanoparticles volume fraction do not have significant effects on $U$. The slip coefficient ($B$) leads to generate the slip velocity at $Y = 0$ and $Y = 1$ which is well obvious in Fig. 6. However, it has the maximum value at entrance and then decreases along the microchannel. In contrary of usual flows in channels (at macro scales), the maximum value of $U$ is less than 1.5 in fully developed region due to slip velocity on the walls.

Fig. 7 shows the dimensionless temperature profiles, $\theta = T/T_i$, along the microchannel at $B = 0.005$ and for $\varphi = 0$ and $\varphi = 0.04$. The nanofluid temperature increases along the microchannel so that at $x = 0.16$ L, its temperature approaches almost to that of the wall. Moreover, the significant temperature jump is observed at inlet which decreases moderately along the walls to the outlet. However, there is very small value of temperature jump in fully developed region.

The effects of $\varphi$ on $Nu_X$ and temperature jump ($\theta_s$) along the microchannel wall are shown in Figs. 8 and 9 at $B = 0.005$ for $\varphi = 0$, $\varphi = 0.02$ and $\varphi = 0.04$, respectively. $Nu_X$ and $\theta_s$ have largest value at entrance and then start to decrease asymptotically along walls and approach constant values. Moreover, they increase with $\varphi$. However, this phenomenon is more significant for Nu. Fig. 9 portraits significant values of temperature jump especially around the entrance region, which has the most temperature gradient near the wall. Thus, more accurate results can be obtained near the walls, if the temperature jump and its effects are taken into account. However, in previous works the temperature jump had been ignored [44,45,48].

### 5.2. Effects of B (dimensionless slip coefficient)

Figs. 10 and 11 show $U$ and $\theta$ along the microchannel at $B = 0.01$ and $B = 0.02$ for $\varphi = 0.04$, respectively. It can be observed that larger $B$ corresponds to larger slip velocity as well as temperature jump on the walls, especially at the entrance region.

The streamlines and isotherms of nanofluid inside the microchannel are shown in Fig. 12 at $B = 0.005$ (line) and $B = 0.02$
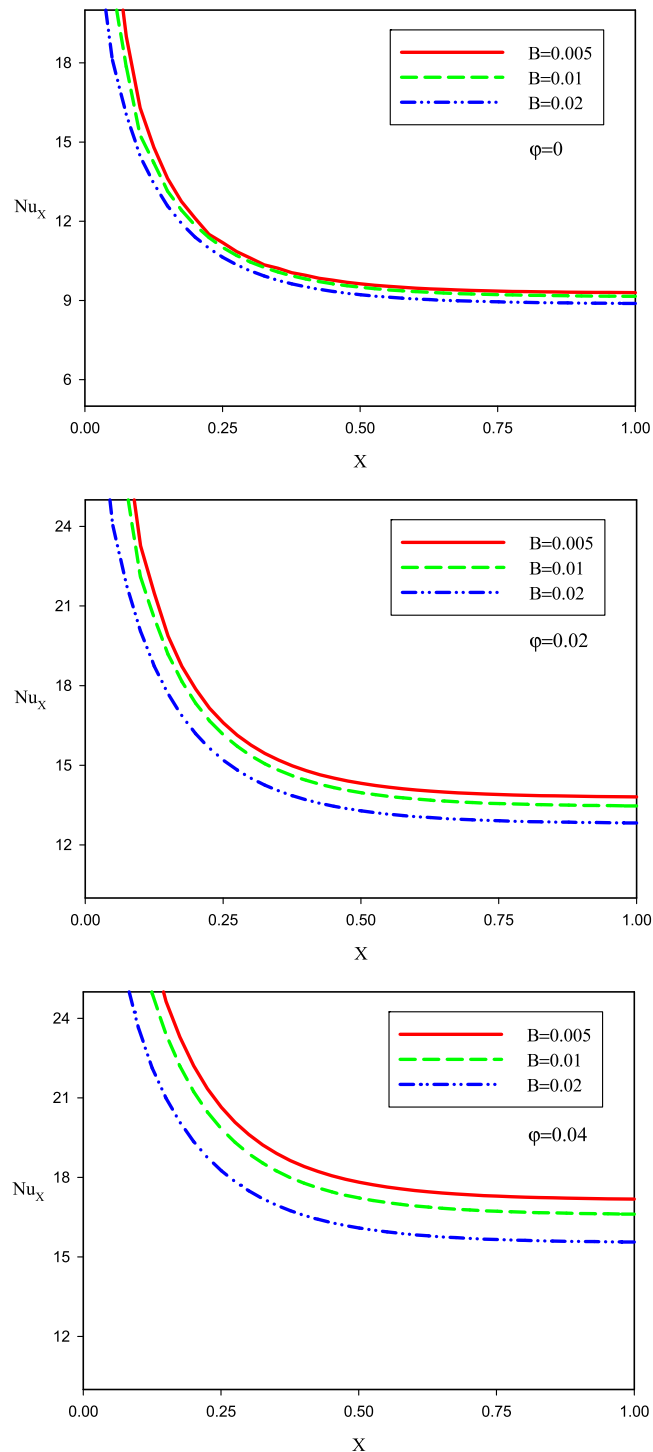


**Fig. 13.** The variations of $Nu_X$ along the microchannel wall at $B = 0.005$, $B = 0.01$ and $B = 0.02$ for $\varphi = 0$, $\varphi = 0.02$ and $\varphi = 0.04$.

(dash) for $\varphi = 0.04$. Nanofluid enters the microchannel from the left and after cooling the walls, it leaves from the right side. So,
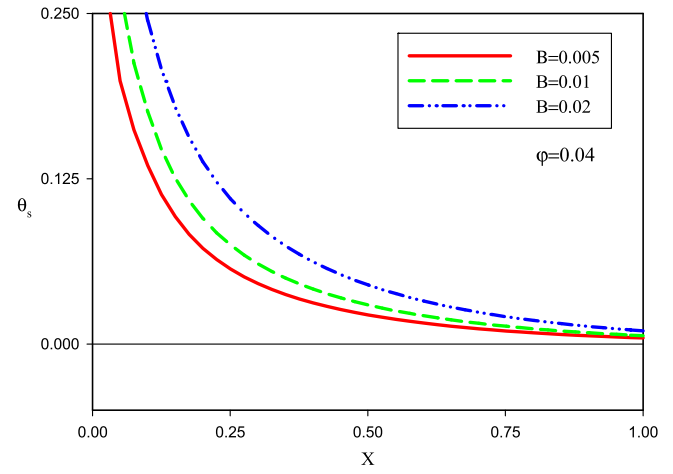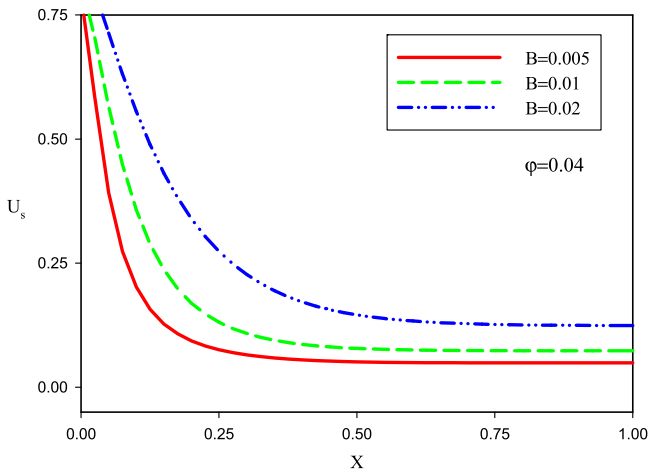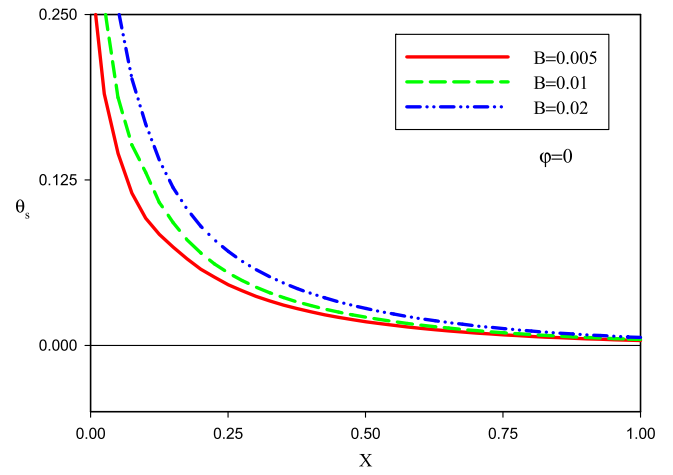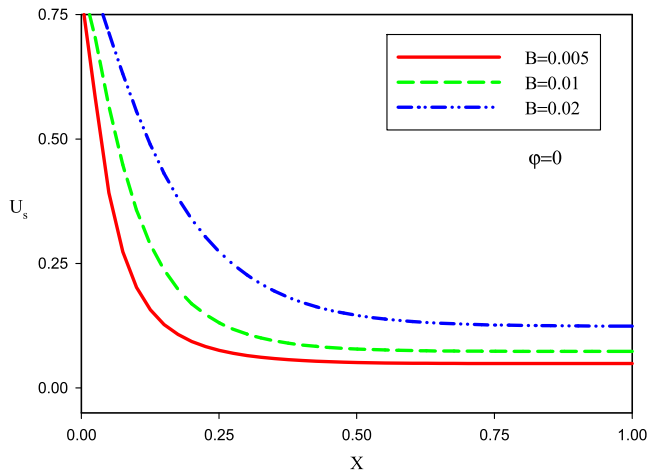
**Fig. 14.** $U_s$ along the microchannel wall at $B = 0.005$, $B = 0.01$ and $B = 0.02$ for $\varphi = 0$ and $\varphi = 0.04$.



**Fig. 15.** $\theta_s$ along the microchannel wall at $B = 0.005$, $B = 0.01$ and $B = 0.02$ for $\varphi = 0$ and $\varphi = 0.04$.

there will be symmetric and horizontal streamlines along the microchannel.

Fig. 13 demonstrates the variations of $Nu_X$ along the microchannel walls at $B = 0.005$, $B = 0.01$ and $B = 0.02$ for $\varphi = 0$, $\varphi = 0.02$ and $\varphi = 0.04$. It can be seen that Nu increases with $\varphi$; but decreases with $B$. Temperature gradient between the nanofluid particles on the wall and their neighbor ones adjacent to the wall, decreases at larger $B$; as a result Nu would have the less amount at recent case.

The variations of $U_s$ and $\theta_s$ along the microchannel's walls at $B = 0.005$, $B = 0.01$ and $B = 0.02$ for $\varphi = 0.0$ and $\varphi = 0.04$ are represented in Figs. 14 and 15, respectively. It can be observed that at the inlet, the slip velocity and temperature jump start from their maximum values and decrease asymptotically along the wall and approach constant values. The variation of $\varphi$ does not have significant effect on these parameters. However, increasing $B$ leads to increase in both $U_s$ and $\theta_s$.

Nu at the outlet – with different values of $\varphi$ and $B$ – is presented in Fig. 16, which indicates the importance of using nanofluid to increase the heat transfer rate. Using 2% of Cu nanoparticles leads to increase almost 30% of outlet Nu at $B = 0.005$. This increase would be almost 45% for using 4% of Cu ones.

## 6. Conclusion

An in-house, FORTAN code based on a double population LBM–BGK method was utilized to simulate laminar forced convection heat transfer of Cu–water nanofluid in a microchannel. The
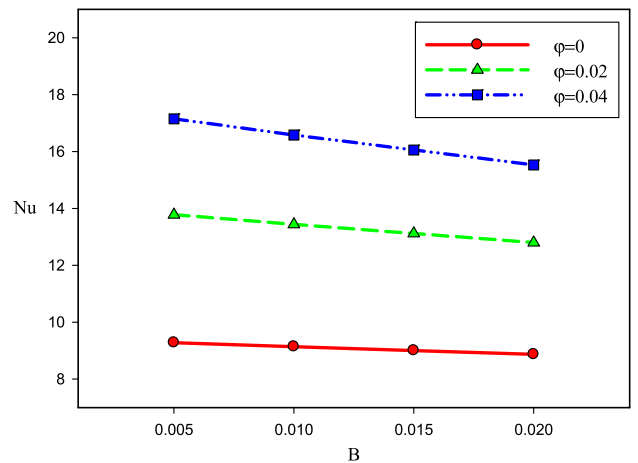


**Fig. 16.** Nanofluid outlet Nu with different values of $\varphi$ and $B$.

effects of different volume fractions of copper nanoparticles and slip coefficient were investigated on the slip velocity, temperature jump and Nusselt number for Re = 0.01. Nanofluid slip velocity and temperature jump were simulated by the lattice Boltzmann method, for the first time at present study.

According to the simulation results, the fully developed condition was observed after the short entrance length, equals $X = 0.08\ L$. Nanofluid temperature increased along the microchannel

so that at $x = 0.16$ L, its temperature approached the walls one. It was particularly noted that $Nu_x$, $\theta_s$ and $U_s$ have largest values at the entrance and then they decrease asymptotically along the walls and approach constant values.

The simulation results confirmed that $\varphi$ did not have significant effects on $U$; however higher $\varphi$ corresponds to larger Nu. Using 2% of Cu nanoparticles led to increase almost 30% of outlet Nu showing the appropriate performance of nanofluid in a microchannel.

Moreover, it was noted that larger value of B corresponds to smaller value of Nu and larger values of $U_s$ and $\theta_s$. Significant value of temperature jump was seen along the microchannel walls especially at the entrance region which has the most temperature gradient between the walls and nanofluid. Therefore, to obtain more accurate results, $\theta_s$ and its effects should be considered, in contrary to the previous works where it had been ignored.

As a result, to increase Nu in micro liquid flows, it is recommended to use nanofluid with $\varphi = 4\%$ and at low values of slip coefficient as like $B = 0.005$. However, the effect of $\varphi$ is more pronounced compared to B.

# References

[1] H.P. Kavehpour, M. Faghri, Y. Asako, Effects of compressibility and rarefaction on gaseous flows in microchannels, Numer. Heat Transfer A 32 (1997) 677–696.

[2] K. Hooman, A superposition approach to study slip-flow forced convection in straight microchannels of uniform but arbitrary cross-section, Int. J. Heat Mass Transfer 51 (2008) 3753–3762.

[3] K. Hooman, H. Gurgenci, Effects of temperature-dependent viscosity on forced convection inside a porous medium, Transp. Porous Media 75 (2) (2008) 249–267.

[4] Marjan Goodarzi, M.R. Safaei, A. Karimipour, K. Hooman, M. Dahari, S.N. Kazi, E. Sadeghinezhad, Comparison of the finite volume and lattice boltzmann methods for solving natural convection heat transfer problems inside cavities and enclosures, Abstr. Appl. Anal. (2014) http://dx.doi.org/10.1155/2014/762184. Article ID 762184.

[5] N.T. Nguyen, S.T. Wereley, Fundamentals and Applications of Microfluidics, Second ed., Artech House, Norwood, 2006.

[6] K. Hooman, Entropy generation for microscale forced convection: Effects of different thermal boundary conditions, velocity slip, temperature jump, viscous dissipation, and duct geometry, Int. Commun. Heat Mass Transfer 34 (8) (2007) 945–957.

[7] S. Naris, D. Valougeorgis, Rarefied gas flow in a triangular duct based on a boundary fitted lattice, Eur. J. Mech. Fluids 27 (2008) 810–822.

[8] S. Pantazis, D. Valougeorgis, Rarefied gas flow through a cylindrical tube due to a small pressure difference, Eur. J. Mech. Fluids 38 (2013) 114–127.

[9] K. Hooman, F. Hooman, M. Famouri, Scaling effects for flow in micro-channels: Variable property, viscous heating, velocity slip, and temperature jump, Int. Commun. Heat Mass Transfer 36 (2) (2009) 192–196.

[10] G. Bird, Molecular gas dynamics and the direct simulation of gas flows, Oxford, 1994.

[11] E.S. Oran, C.K. Oh, B.Z. Cybyk, Direct simulation Mont Carlo: recent advances and applications, Annu. Rev. Fluid Mech. 30 (1998) 403–441.

[12] C.Y. Lim, C. Shu, X.D. Niu, Y.T. Chew, Application of lattice Boltzmann method to simulate microchannel flows, Phys. Fluids 14 (2002) 2299–2308.

[13] C. Shu, X.D. Niu, Y.T. Chew, A lattice Boltzmann kinetic model for microflow and heat transfer, J. Stat. Phys. 121 (2005) 239–255.

[14] V. Sofonea, R.F. Sekerka, Boundary conditions for the upwind finite difference Lattice Boltzmann model: evidence of slip velocity in micro-channel flow, J. Comput. Phys. 207 (2005) 639–659.

[15] Y.H. Zhang, R.S. Qin, Y.H. Sun, R.W. Barber, D.R. Emerson, Gas flow in microchannels — a lattice Boltzmann method approach, J. Stat. Phys. 121 (2005) 257–267.

[16] W.C. Hung, Y. Ru, A numerical study for slip flow heat transfer, Appl. Math. Comput. 173 (2006) 1246–1264.

[17] A. Karimipour, M.H. Esfe, M.R. Safaei, D.T. Semiromi, S. Jafari, S.N. Kazi, Mixed convection of copper–water nanofluid in a shallow inclined lid driven cavity using the lattice Boltzmann method, Physica A 402 (2014) 150–168.

[18] Z.W. Tian, C. Zou, H.J. Liu, Z.L. Guo, Z.H Liu, C.G. Zheng, Lattice Boltzmann scheme for simulating thermal micro-flow, Physica A 385 (2007) 59–68.

[19] H. Babovsky, A numerical model for the Boltzmann equation with applications to micro flows, Comput. Math. Appl. 58 (2009) 791–804.

[20] S. Chen, Z. Tian, Simulation of microchannel flow using the lattice Boltzmann method, Physica A 388 (2009) 4803–4810.

[21] P.L. Bhatnagar, E.P. Gross, M. Krook, A model for collision process in gases. I. Small amplitude processes in charged and neutral one-component system, Phys. Rev. 94 (1954) 511–522.

[22] S. Succi, The lattice Boltzmann equation for fluid dynamics and beyond, first ed., Oxford, 2001.

[23] S. Chen, Lattice Boltzmann method for slip flow heat transfer in circular microtubes: extended Graetz problem, Appl. Math. Comput. 217 (2010) 3314–3320.

[24] S. Chen, Z. Tian, Entropy generation analysis of thermal micro-Couette flows in slip regime, Int. J. Therm. Sci. 49 (2010) 2211–2221.

[25] X. He, S. Chen, G.D. Doolen, A novel thermal model for the lattice Boltzmann method in incompressible limit, J. Comput. Phys. 146 (1998) 282–300.

[26] A. D'Orazio, S. Succi, C. Arrighetti, Lattice Boltzmann simulation of open flows with heat transfer, Phys. Fluids 15 (2003) 2778–2781.

[27] A. D'Orazio, M. Corcione, G.P. Celata, Application to natural convection enclosed flows of a lattice Boltzmann BGK model coupled with a general purpose thermal boundary condition, Int. J. Therm. Sci. 43 (2004) 575–586.

[28] A. Karimipour, A.H. Nezhad, A. D'Orazio, E. Shirani, The effects of inclination angle and Prandtl number on the mixed convection in the inclined lid driven cavity using lattice Boltzmann method, J. Theoret. Appl. Mech. 51 (2) (2013) 447–462.

[29] L. Szalmas, Multiple-relaxation time lattice Boltzmann method for the finite Knudsen number region, Physica A 379 (2007) 401–408.

[30] M. Goodarzi, M.R. Safaei, H.F. Oztop, A. Karimipour, E. Sadeghinezhad, M. Dahari, S.N. Kazi, N. Jomhari, Numerical study of entropy generation due to coupled laminar and turbulent mixed convection and thermal radiation in an enclosure filled with a semitransparent medium, Sci. World J. (2014) 8. http://dx.doi.org/10.1155/2014/761745. Article ID 761745.

[31] F. Verhaeghe, L.S. Luo, B. Blanpain, Lattice Boltzmann modeling of microchannel flow in slip flow regime, J. Comput. Phys. 228 (2009) 147–157.

[32] S. Chen, Z. Tian, Simulation of thermal micro-flow using lattice Boltzmann method with Langmuir slip model, Int. J. Heat Fluid Flow 31 (2010) 227–235.

[33] Z. Tian, S. Chen, C.G. Zheng, Lattice Boltzmann simulation of gaseous finite-Kundsen microflows, Internat. J. Modern Phys. C 21 (2010) 769–783.

[34] A. Karimipour, A.H. Nezhad, A. D'Orazio, E. Shirani, Investigation of the gravity effects on the mixed convection heat transfer in a microchannel using lattice Boltzmann method, Int. J. Therm. Sci. 54 (2012) 142–152.

[35] H. Khorasanizadeh, M. Nikfar, J. Amani, Entropy generation of Cu–water nanofluid mixed convection in a cavity, Eur. J. Mech. B Fluids 37 (2013) 143–152.

[36] A.K. Santra, S. Sen, N. Chakraborty, Study of heat transfer due to laminar flow of copper–water nanofluid through two isothermally heated parallel plates, Int. J. Therm. Sci. 48 (2009) 391–400.

[37] M. Goodarzi, M.R. Safaei, G. Ahmadi, K. Vafai, M. Dahari, N. Jomhari, S.N. Kazi, An investigation of laminar and turbulent nanofluid mixed convection in a shallow rectangular enclosure using a two-phase mixture model, Int. J. Therm. Sci. 75 (2014) 204–220.

[38] H. Togun, M.R. Safaei, R. Sadri, S.N. Kazi, A. Badarudin, K. Hooman, E. Sadeghinezhad, Heat transfer to turbulent and laminar Cu/water flow over a backward-facing step, Appl. Math. Comput. 239 (2014) 153–170.

[39] G.A. Sheikhzadeh, A. Arefmanesh, M.H. Kheirkhah, R. Abdollahi, Natural convection of Cu–water nanofluid in a cavity with partially active side walls, Eur. J. Mech. B Fluids 30 (2011) 166–176.

[40] M.R. Safaei, M. Goodarzi, M. Mohammadi, Numerical modeling of turbulence mixed convection heat transfer in air filled enclosures by finite volume method, Int. J. Multiphys. 5 (2011) 307–324.

[41] A. Karimipour, A.H. Nezhad, A. Behzadmehr, S. Alikhani, E. Abedini, Periodic mixed convection of a nanofluid in a cavity with top lid sinusoidal motion, Proc. IMechE Part C: J. Mech. Eng. Sci. 225 (2011) 2149–2160.

[42] M.H. Esfe, M. Akbari, D. Toghraie, A. Karimipour, M. Afrand, Effect of nanofluid variable properties on mixed convection flow and heat transfer in an inclined two-sided lid-driven cavity with sinusoidal heating on sidewalls, Heat Transfer Res. 45 (2014) 409–432.

[43] M.H. Esfe, A.A.A. Arani, A. Karimipour, S.S.M. Esforjani, Numerical simulation of natural convection around an obstacle placed in an enclosure filled with different types of nanofluids, Heat Transfer Res. 45 (2014) 279–292.

[44] S.M. Aminossadati, A. Raisi, B. Ghasemi, Effects of magnetic field on nanofluid forced convection in a partially heated microchannel, Int. J. Non-Linear Mech. 46 (2011) 1373–1382.

[45] M. Kalteh, A. Abbassi, M. Saffar-Avval, J. Harting, Eulerian–Eulerian two-phase numerical simulation of nanofluid laminar forced convection in a microchannel, Int. J. Heat Fluid Flow 32 (2011) 107–116.

[46] M. Mital, Semi-analytical investigation of electronics cooling using developing nanofluid flow in rectangular microchannels, Appl. Therm. Eng. 52 (2013) 321–327.

[47] M. Mital, Analytical analysis of heat transfer and pumping power of laminar nanofluid developing flow in microchannels, Appl. Therm. Eng. 50 (2013) 429–436.

[48] A. Raisi, B. Ghasemi, S.M. Aminossadati, A numerical study on the forced convection of laminar nanofluid in a microchannel with both slip and no-slip conditions, Numer. Heat Transfer A 59 (2011) 114–129.

[49] A. Tamayol, K. Hooman, Slip-flow in microchannels of non-circular cross sections, J. Fluids Eng. 133 (9) (2011) 091202-1–091202-8.

[50] K. Hooman, A. Ejlali, Effects of viscous heating, fluid property variation, velocity slip, and temperature jump on convection through parallel plate and circular microchannels, Int. Commun. Heat Mass Transfer 37 (1) (2010) 34–38.

[51] L. Zhou, Y. Xuan, Q. Li, Multiscale simulation of flow and heat transfer of nanofluid with lattice Boltzmann method, Int. J. Multiphase Flow 36 (2010) 364–374.

[52] M.H. Esfe, S.S.M. Esforjani, M. Akbari, A. Karimipour, Mixed-convection flow in a liddriven square cavity filled with a nanofluid with variable properties: effect of the nanoparticle diameter and of the position of a hot obstacle, Heat Transfer Res. 45 (2014) 563–578.

[53] F.H. Lai, Y.T. Yang, Lattice Boltzmann simulation of natural convection heat transfer of Al2O3/water nanofluids in a square enclosure, Int. J. Therm. Sci. 50 (2011) 1930–1941.

[54] Y. Guo, D. Qin, S. Shen, R. Bennacer, Nanofluid multi-phase convective heat transfer in closed domain: Simulation with lattice Boltzmann method, Int. Commun. Heat Mass Transfer 39 (2012) 350–354.

[55] C. Ay, C.W. Young, C.F. Young, Application of lattice Boltzmann method to the fluid analysis in a rectangular microchannel, Comput. Math. Appl. 64 (2012) 1065–1083.

[56] Y.T. Yang, F.H. Lai, Numerical study of flow and heat transfer characteristics of alumina-water nanofluids in a microchannel using the lattice Boltzmann method, Int. Commun. Heat Mass Transfer 38 (2011) 607–614.

[57] Y. Xuan, Q. Li, Investigation on convective heat transfer and flow features of nanofluids, ASME J. Heat Transfer 125 (2003) 151–155.

[58] H.C. Brinkman, The viscosity of concentrated suspensions and solutions, J. Chem. Phys. 20 (1952) 571–581.

[59] C.H. Chon, K.D. Kihm, S.P. Lee, S.U.S. Choi, Empirical correlation finding the role of temperature and particle size for nanofluid ($Al_2O_3$) thermal conductivity enhancement, Appl. Phys. Lett. 87 (2005) 153107.

[60] S. Chapman, T.G. Cowling, The Mathematical Theory of Non-uniform Gases, third ed., Cambridge, 1999.

[61] Y. Qian, D. Humie'res, P. Lallemand, Lattice BGK models for Navier–Stokes equation, Europhys. Lett. 17 (1992) 479–484.

[62] X.D. Niu, C. Shu, Y.T. Chew, A thermal lattice Boltzmann model with diffuse scattering boundary condition for micro thermal flows, Comp. Fluids 36 (2007) 273–281.

[63] A. D'Orazio, S. Succi, Simulating two-dimensional thermal channel flows by means of a lattice Boltzmann method with new boundary conditions, Future Gener. Comput. Syst. 20 (2004) 935–944.

[64] Q. Zou, X. He, On pressure and velocity boundary conditions for the lattice Boltzmann BGK model, Phys. Fluids 9 (1997) 1591–1599.

[65] A.A. Alamyane, A.A. Mohamad, Simulation of forced convection in a channel with extended surfaces by the lattice Boltzmann method, Comput. Math. Appl. 59 (2010) 2421–2430.

[66] M. Gad-el-Hak, Flow physics in MEMS, Rev. Mech. Ind. 2 (2001) 313–341.

[67] P.A. Thompson, S.M. Troian, A general boundary condition for liquid flow at solid surfaces, Phys. Rev. Lett. 63 (1997) 766–769.

[68] G.D. Ngoma, F. Erchiqui, Heat flux and slip effects on liquid flow in a microchannel, Int. J. Therm. Sci. 46 (2007) 1076–1083.

[69] G. Karniadakis, A. Beskok, Micro flows: fundamentals and simulation, New York, 2002.

[70] S. Succi, Mesoscopic modelling of slip motion at fluid-solid interfaces with heterogeneous catalysis, Phys. Rev. Lett. 89 (2002).

[71] A. Akbarinia, M. Abdolzadeh, R. Laur, Critical investigation of heat transfer enhancement using nanofluids in microchannels with slip and non-slip flow regimes, Appl. Therm. Eng. 31 (2011) 556–565.